robotics

MDPI

Article

Design of a Three-Degree of Freedom Planar Parallel Mechanism for the Active Dynamic Balancing of Delta Robots

Christian Mirz [1,*], Mathias Hüsing [1], Yukio Takeda [2] and Burkhard Corves [1]

[1] Institute of Mechanism Theory, Machine Dynamics and Robotics, RWTH Aachen University, 52062 Aachen, Germany
[2] Department of Mechanical Engineering, School of Engineering, Tokyo Institute of Technology, Tokyo 152-8550, Japan
* Correspondence: mirz@igmr.rwth-aachen.de

Abstract: Delta robots are the most common parallel robots for manipulation tasks. In many industrial applications, they must be operated at reduced speed, or dwell times have to be included in the motion planning, to prevent frame vibrations. As a result, their full potential cannot be realized. Against this background, this publication is concerned with the mechanical design of an active dynamic balancing unit for the reduction of frame vibrations. In the first part of this publication, the main design requirements for an active dynamic balancing mechanism are discussed, followed by a presentation of possible mechanism designs. Subsequently, one the most promising mechanisms is described in detail and its kinematics and dynamics equations are derived. Finally, the dimensions of a prototype mechanism designed to experimentally validate the concept of active dynamic balancing are defined using the example of Suisui Bot, a low-cost Delta robot.

Keywords: dynamic balancing; vibration reduction; delta robot; pick and place; parallel mechanism; parallel robot; planar mechanism; high speed manipulation; handling task

check for updates

Citation: Mirz, C.; Hüsing, M.; Takeda, Y.; Corves, B. Design of a Three-Degree of Freedom Planar Parallel Mechanism for the Active Dynamic Balancing of Delta Robots. *Robotics* **2024**, *13*, 129. https://doi.org/10.3390/robotics13090129

Academic Editors: Dan Zhang and Raffaele Di Gregorio

Received: 28 June 2024
Revised: 4 August 2024
Accepted: 25 August 2024
Published: 27 August 2024

Copyright: © 2024 by the authors. Licensee MDPI, Basel, Switzerland. This article is an open access article distributed under the terms and conditions of the Creative Commons Attribution (CC BY) license (https://creativecommons.org/licenses/by/4.0/).

1. Introduction

Dynamic manipulation tasks, as found in the packaging industry, demand lightweight, stiff robotic systems, with a high payload-to-weight ratio, to achieve both energy efficiency and high positioning accuracy. Given these requirements, parallel robots are particularly well suited due to their architecture with base-fixed actuators and, hence, low moving mass [1]. The most common parallel robots for these tasks are Delta robots [1]. In many industrial applications, they must be operated at reduced speed, or dwell times have to be included in the motion planning, to allow frame vibrations to decay and hereby prevent unacceptably high vibrations from building up [2]. Otherwise, the vibrations reduce the accuracy of the robot, can cause fatigue and wear in its mechanical elements, cause noise, or even affect surrounding machines [2–4]. As a result, the full potential of Delta robots cannot be realized. The vibrations can be explained by the high speeds and accelerations required to achieve the desired short cycle times. These cause high inertia forces and moments, which act on the frame. This problem is exacerbated by the mostly slim and high structure of the frames. A typical setup of a Delta robot, including the coordinate system (COS) used in the remainder of this publication, is shown in Figure 1. Given this geometry, they tend to vibrate laterally, especially during horizontal robot motions, typical for pick-and-place tasks.

Methods for the reduction of frame vibrations may be classified as software, hardware, and hybrid approaches. Software-based approaches comprise trajectory planning methods that aim to either minimize the excitation of natural frequencies, e.g., ref. [5,6], to minimize the shaking forces/moments, e.g., ref. [7], or to suppress residual vibrations, e.g., refs. [8–10]. A necessary condition to achieve both tool center point (TCP) control and vibration suppression is a sufficient kinematic/dynamic redundancy [7], to control the center of mass (CoM) and TCP

position independently, which is not met by Delta robots. Consequently, in the case of Delta robots, at best, trajectory planning methods achieve vibration minimization or elimination of residual vibrations after the robot motion is completed.

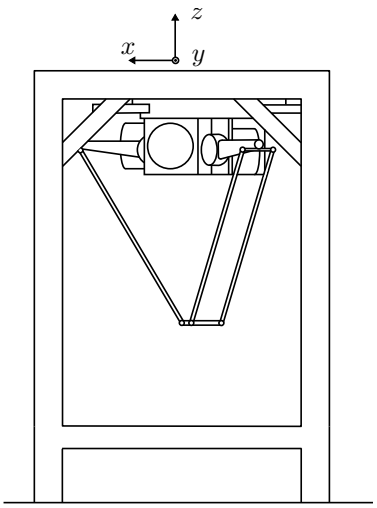


Figure 1. Typical setup of a Delta robot.

The goal of hardware and hybrid methods is to maintain a constant linear and angular momentum by adding additional actively or passively driven counterweights and counter rotating inertia. This is referred to as dynamic balancing. If the counterweights and inertia are directly or indirectly (e.g., by additional kinematic chains) driven by the manipulator's actuators, it may be categorized as a hardware-based approach. In the case of an active actuation (i.e., active dynamic balancing) it may be considered a hybrid approach. Both can be used for vibration prevention. In [2], van der Wijk et al. present a dynamically balanced Delta robot with respect to inertial forces by adding three counterweights and two additional links. As a result, the moving mass of the robot increases approximately three-fold. This is accompanied by an increase of the driving torques. The use of an active balancing mechanism has the advantage that it can be adapted in the software to a wide range of tasks and can be applied to different robot models of similar size and performance without hardware modifications. In addition, the handling object's mass can be taken into account. A disadvantage is that an additional control system and actuators are needed, which increases the design complexity.

Despite these advantages, comparably little literature is found regarding active dynamic balancing [11], as active research on this method is relatively young [12] and covers mostly theoretical studies. In [11], van der Wijk et al. presented the first active dynamic balancing unit [13]. It was designed as an $\underline{R}RRR\underline{R}$ mechanism, i.e., a five-bar linkage with an actively driven counterrotating counterweight attached to its TCP. In this representation, $\underline{R}RRR\underline{R}$ refers to a parallel mechanism with two $\underline{R}R$ kinematic chains, each with two revolute joints, connected to each other by a revolute joint. The underlined joints are actuated. This mechanism was used to balance a planar gantry manipulator suspended by three cables [14]. The balancing mechanism was controlled based on the dynamics of the manipulator and the balancing mechanism [11]. Here, only the counterrotating counterweight was taken into account; the mass and inertia of the five-bar linkage are neglected to simplify the dynamics equations. The validity of this method has been experimentally proven [14]. An example of a passively force-balanced mechanism, in combination with one actively driven counter inertia used for moment balancing, was presented in [15], applied to a planar $\underline{R}RRR\underline{R}$ parallel robot [2]. A similar design was presented by Wang et al. in [16], where the authors proposed to use a planar $\underline{P}RRR\underline{P}$ mechanism, the linearly actuated equivalent of the five-bar linkage, with a counterrotating counterweight attached to its TCP. In this notation, P represents a prismatic joint. Later, Wang et al. [12] proposed a

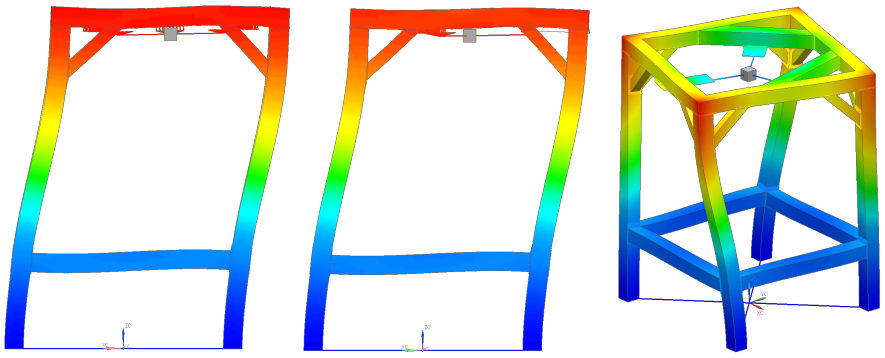
second design consisting of three independently rotating one-link mechanisms ($\underline{R}$), for the dynamic balancing of planar three-DoF manipulators.

The present publication presents the design of a novel planar three-DoF balancing mechanism with minimum mass and inertia, designed for the active dynamic balancing of Delta robots. The balancing mechanism presented in this publication was designed according to the engineering guideline VDI 2221 [17]. It proposes a general process of the product design consisting of eight stages. The first step in the design of a technical product is the clarification of the problem task. The result of this step is a list of requirements, as will be presented in Section 2. This is followed by developing and selecting design concepts. For this purpose, the required functions and their structure are defined. A function-oriented approach can help to expand the search space and support the search for alternative or innovative solution principles and also form the basis for common design methods [17]. The functions define what the product or its components should do. They are described in a simple "object–verb form" (e.g., "constrain motion") [18]. The next step is to search for solution principles for the defined functions, e.g., using conventional methods such as literature and patent research as well as the analysis of natural systems, discursive methods using classification schemes, or intuitive methods like brainstorming [18]. These functions and their solution principles are introduced in Section 3, followed by a detailed presentation of one of the most promising balancing mechanisms. For this mechanism, the kinematics and dynamics equations are derived in Section 4. Finally, in Section 5, the dimensions of a prototype mechanism designed to experimentally validate the concept of active dynamic balancing are defined.

2. Design Requirements

In [19], a detailed analysis of the shaking forces and moments caused by Delta robots and the interaction between these forces/moments and the dynamics of typical industrial robot frames was performed. The results of this analysis form the basis for the mechanism design and are therefore briefly summarized below.

Due to the mostly slender and high structure of the frames, the first three natural frequencies belong to eigenmodes describing a horizontal translation in the xy-plane and a rotation around the z-axis, as shown in Figure 2.



1. Eigenmode 31.7 Hz | 2. Eigenmode 31.8 Hz | 3. Eigenmode 49.2 Hz

Figure 2. Eigenmodes and natural frequencies of a typical Delta robot frame.

The motion of the first two mode shapes coincides with the direction of the dominant shaking forces, which occur in the xy-plane and coincide with the main direction of motion of the robots. As a result, simulations and experiments conducted in [19] to analyze the frame vibrations indicate a dominance of vibrations in the horizontal plane. Against this background, the balancing mechanism is designed to eliminate the vibration forces in the xy-plane. If the lines of action of the balancing forces do not cross the center of the frame, they lead to additional shaking moments about the z-axis. These moments would excite

the third, rotational eigenmode of the frame. To compensate for these parasitic moments, moments about the z-axis are also compensated.

In addition to the requirements derived from the analysis of the vibration characteristics of Delta robot frames, we will now examine design requirements that originate from the active dynamic balancing process itself. These requirements pertain to the following:

- Parasitic shaking forces and moments: If the shaking forces are not collinear with the balancing forces, force balancing will result in additional parasitic shaking moments. This is shown schematically in Figure 3a. The motion of the counterweight's and the robot's CoM are parallel but not colinear. Even if the sum of the inertia forces is zero, they create a force couple around the attachment point, which leads to a parasitic shaking moment.
- High ratio of counterweight's mass to stationary mass: The mass of the balancing mechanism placed on top of the robot's frame inevitably leads to a reduction in the frame's natural frequencies, which could make the system more susceptible to frame vibrations. It also places higher demands on the structural rigidity of the frame to prevent unacceptable static deflections due to gravitational loads. Therefore, the ratio of the counterweight's mass and all moving masses that contribute to the balancing, to the stationary mass of the balancing mechanism, which does not participate in balancing (e.g., base mass), should be as high as possible.
- Kinematics and Dynamics Complexity: Most control designs require the solution of kinematics and dynamics equations for each time step. Thus, complex, nonlinear dynamics that can only be solved numerically place high demands on the control hardware. To allow the use of low-performance, low-cost control hardware, it is desirable to design a balancing mechanism with linear kinematics and dynamics equations.
- Stiffness of the connection to the robot: If the balancing mechanism is mounted far from the robot mounting point, the balancing forces/moments must be transmitted through the frame. The compliance of the frame can cause non-negligible dynamic effects in the transmission of forces/moments to the robot base. It is therefore desirable to have a high rigidity in the connection between the robot and the balancing mechanism.
- Size: To avoid collisions and a high adaptability to different frame designs, it is desirable to keep the balancing mechanism as small as possible. At the same time, if the counterweight is also used as a counter rotating inertia, a large diameter of the counterweight is desirable to keep the mass low while achieving a high inertia [20].
- Enhancement Effects: When a rotating actuator is used to drive a counterrotating inertia, the direction of rotation of the actuator and the counterrotating inertia should coincide. In this case, the actuator inertia participates in the moment balancing [11]. This and similar enhancements should be used when applicable.
- Costs: Costs include both operating and acquisition costs. The sum of the two must be offset by the increased productivity provided by shorter cycle times.

The power requirement of the balancing unit depends on the mass and moment of inertia of the counterweight. For simplicity and without loss of generality, this shall be shown on the example of a one-dimensional balancing task. The acceleration, $\ddot{x}_b$, of the counterweight, m_b, can be calculated by the equilibrium of forces:

$$f_s = -\ddot{x}_m m_m = \ddot{x}_b m_b \,. \tag{1}$$

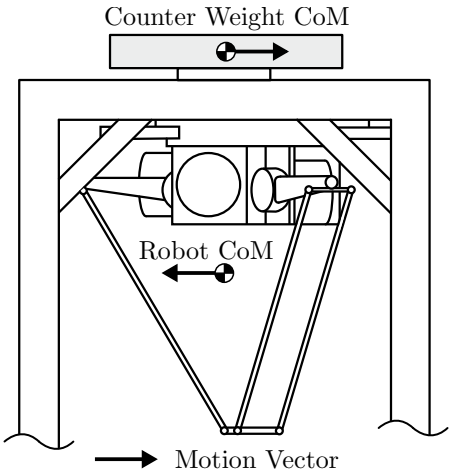
Here, m_m denotes the total mass and $\ddot{x}_m$ the CoM acceleration of the mechanism that is to be balanced. Consequently, f_s represents the shaking force caused by the manipulator. Dividing by the counterweight's mass, m_b, and substitution with $\lambda = \frac{m_m}{m_b}$ yields

$$\ddot{x}_b = -\ddot{x}_m \lambda, \quad \dot{x}_b = -\dot{x}_m \lambda, \quad x_b = -x_m \lambda \,. \tag{2}$$

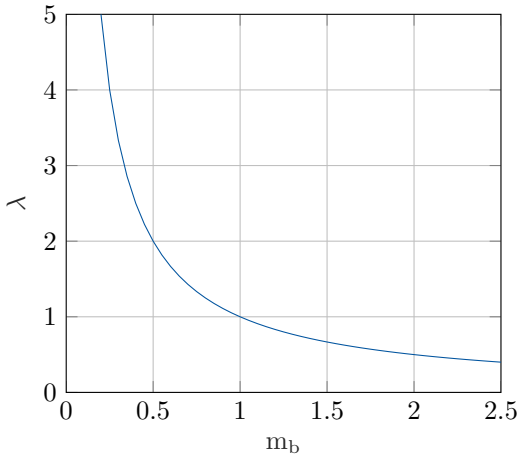
The mechanical power requirement of the balancing unit is defined as

$$p_b = f_s \cdot \dot{x}_b = \ddot{x}_b m_b \dot{x}_b = \ddot{x}_m m_m \dot{x}_m \lambda = \ddot{x}_m \dot{x}_m m_m^2 \left(\frac{1}{m_b} \right). \tag{3}$$

The term $\ddot{x}_m m_m \dot{x}_m$ is fully defined by the mass of the mechanism being balanced and its CoM trajectory. The only variable that can be influenced by the mass of the counterweight is λ. Since λ is a hyperbolic function of the counterweight's mass (cf. Figure 3b), so is the power requirement (3).



(**a**) Non collinear shaking and balancing forces



(**b**) λ values as a function of the counterweight's mass, for $m_m = 1$kg

Figure 3. Illustrations to visualize the origin of parasitic shaking moments and the influence of the counterweight mass on the auxiliary variable λ and thus on the power requirement of the balancing unit.

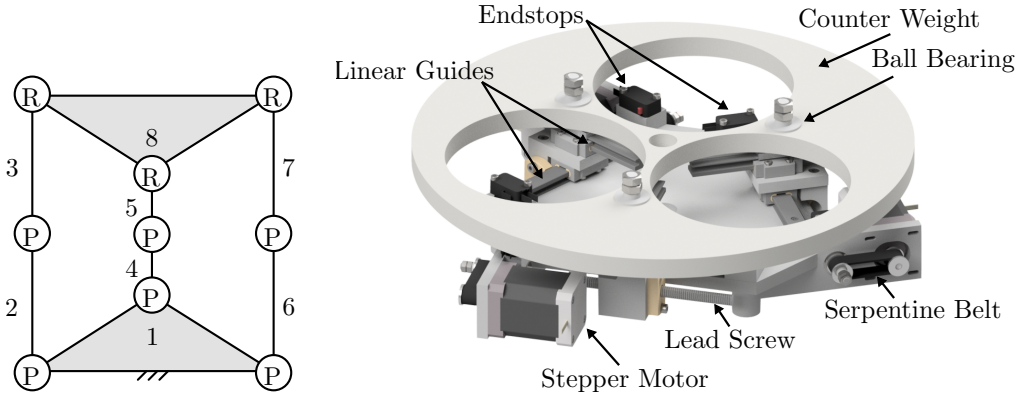
Regarding the target of low operation costs, a high counterweight mass and inertia are favorable. At the same time, a higher mass inevitably leads to a reduction of the frame's natural frequencies and increased demands on its structural stiffness. Therefore, a trade-off between these two goals has to be made.

3. Structural Design of the Balancing Mechanism

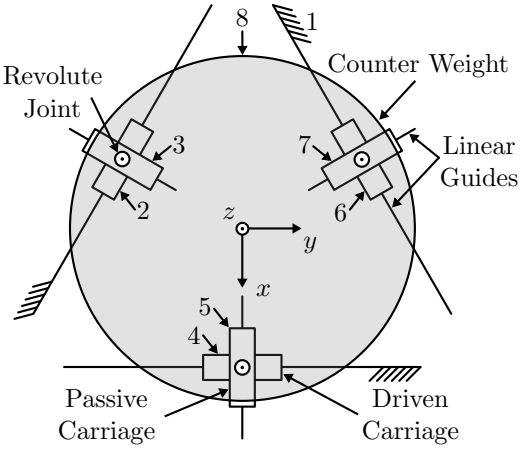
The balancing task was divided into two sub-functions describing the balancing of shaking forces and the balancing of shaking moments. These two functions were further subdivided into a principle mechanism or solution to provide a multi- or unidirectional force/moment, a method to combine these principle mechanisms and to attach them to the robot frame. Following [18], the proposed solutions and their combinations were summarized in a morphological matrix (see Figures A1–A3). In this step, candidate solutions with up to six DoFs were considered. These concepts include novel solutions as well as solutions or adaptations of known solutions from the literature. Examples of the latter include the use of a five-bar mechanism to provide counterbalancing forces in two planar DoF [11], the use of counterrotating eccentric masses as used in the Lanchester balancer [21] and the active three-DoF balancer proposed in [12], or the movement of a fluid or steel balls similar to the solution proposed in [22] to change the mass of the counterweight in a mechanism for the passive balancing of variable payloads. Examples of novel solutions in the context of dynamic balancing are the planar $2-\underline{R}RP$, $3-\underline{P}PR$, and $3-\underline{P}RP$ mechanism (see Figure A2) or a cable-driven parallel robot. Finally, the system concepts were combined into solutions that provide at least three DoF to allow the balancing of forces in the xy plane and moments around the z-axis. These were then evaluated using the criteria presented in the previous section.

A detailed discussion of the characteristics of all the solutions and their combinations is beyond the scope of this publication, so only the most promising concept, which has been further developed, is presented below. The chosen balancing mechanism consists of three identical $\underline{P}PR$ kinematic chains connecting the counterweight to the base, as shown in Figure 4. These kinematic chains consist of two perpendicular guide rails crossing at the center of an actively driven carriage. One of the guide rails is fixed to the base and the

other to the counterweight by means of a revolute joint. The design of this mechanism is inspired by THK Co., Ltd. (Minato City, Tokyo). *CMX* series precision alignment stages [23]. Unlike the balancing mechanism presented here, the *CMX* alignment stages have four *PPR* kinematic chains, only three of which are actuated. The actuators are arranged perpendicular to each other in a square. A variation of this mechanism with $\underline{P}RP$ kinematic chains has been patented by Eidelberg [24]. The triangular arrangement of the balancing mechanism's kinematic chains is similar to the tilt table presented by Kimura in [25].



(**a**) Kinematic structure (**b**) Rendering



(**c**) Schematics

Figure 4. Renderings and schematics of the balancing mechanism.

Using Gruebler's Equation (4), it can be shown that the balancing mechanism has two planar translational and one rotational DoF. Since the mechanism performs planar motions only, Gruebler's equation is given by [26]

$$K = 3 \cdot (n-1) - 3 \cdot g + \sum_{i=1}^{g} k_i = 3 \cdot (8-1) - 3 \cdot 9 + 9 = 3\,, \tag{4}$$

with $n = 8$ being the number of links including the base, $g = 9$ the number of all joints, and $\sum_{i=1}^{g} k_i = 9$ the sum of all joint DoF.

As shown in Figure 4, the triangular arrangement of the kinematic chains results in a small footprint, making the best use of the space at the top of the Delta robot. It also has the same triangular shape as the base of many Delta robot models, which allows it to be mounted directly on the robot, resulting in a direct transmission of the balancing forces to the robot base. In this way, they are compensated at their origin before they can act on the frame. The balancing of shaking forces in the xy-plane and the moments around the z-axis are performed with the same counterweight. This is desirable to minimize the number of additional elements and thus the weight. The radius of the counterweight has

been maximized and cutouts have been made to achieve a high moment of inertia with a low mass. Due to the parallel kinematic design, the mechanism has a low height. This can be seen in Figure 5, which shows the balancing mechanism on a low-cost Delta robot called Suisui Bot, designed by the authors of this publication for experimental validation of vibration reduction methods. Please refer to [27] for more details on the Suisui Bot.

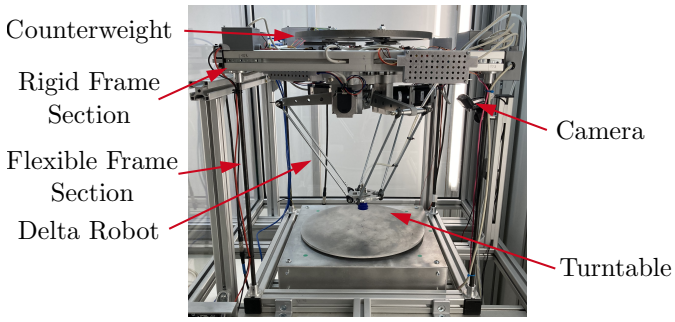


Figure 5. Balancing unit attached to the Suisui Bot.

The counterweight is only 29 mm away from the top of the frame. This low profile allows minimization of the parasitical shaking moments in the xy-plane. Furthermore, the balancing mechanism has, in good approximation, linear kinematics and dynamics, which minimizes the computational effort on the control system (see Section 4.3). Finally, all motors are stationary, minimizing the risk of cable damage. This mechanism was selected due to the combination of the above-mentioned properties, which make it a promising solution for active dynamic balancing. The dimensions of the balancing mechanism are defined in Section 5 after a brief derivation of the inverse dynamics of the mechanism necessary for this step.

4. Kinematics and Dynamics

This section is concerned with the derivation of the balancing mechanism's kinematics and dynamics equations. The geometric center of the counterweight, which coincides with its CoM, will hereafter be referred to as the TCP of the balancing mechanism.

4.1. Inverse Kinematics

The position of the counterweight in respect to the global COS (indicated by the left-sided superscript 0), is represented by the vector ${}^0\boldsymbol{x}$ (compare Figure 6). The global COS is located in the center of the balancing mechanism's base and maintains the same orientation as the COS defined for the Delta robot. The orientation of the TCP with respect to the global COS is represented by the angle ϕ. The unit vector pointing along the base fixed guide rail of the i^{th} kinematic chain $i = \{1, 2, 3\}$ is denoted by ${}^0\boldsymbol{x}_{1,i}$. Similarly, the unit vector ${}^0\boldsymbol{x}_{2,i}$ is perpendicular to ${}^0\boldsymbol{x}_{1,i}$ and points along the second guide rail, which is attached to the counterweight.

Furthermore, the vector pointing from the center of the base to the center of the base fixed guide rail of the i^{th} kinematic chain is denoted by ${}^0\boldsymbol{r}_{b,i}$, and the vector pointing from the center of the counterweight to its revolute joints is given by ${}^0\boldsymbol{r}_{p,i}$. The kinematic chains are arranged uniformly distributed by an angle of 120° on the base radius r_b, as are the revolute joints connected to the counterweight on the radius r_p. The loop closure equation for the i^{th} kinematic chain in the global COS is given as

$$ {}^0\boldsymbol{x} = {}^0\boldsymbol{r}_{b,i} + x_{1,i}\,{}^0\boldsymbol{x}_{1,i} + x_{2,i}\,{}^0\boldsymbol{x}_{2,i} - {}^0\boldsymbol{r}_{p,i}\,. \tag{5} $$

Here, $x_{1,i}$ and $x_{2,i}$ denote scalar scaling factors, representing the position of the carriage on the base-fixed guide rail ${}^0\boldsymbol{x}_{1,i}$ and the position of the revolute joint with respect to the

carriage. Additionally, $\alpha_i = (i-1)\frac{2\pi}{3}$ denotes the attachment angle of the i^{th} kinematic chain with respect to the x-axis of the global COS. Thus,

$$ {}^0\boldsymbol{r}_{b,i} = r_b \boldsymbol{R}_{z,\alpha} (1,0,0)^T \tag{6} $$

$$ {}^0\boldsymbol{r}_{p,i} = r_p \boldsymbol{R}_{z,\alpha+\phi} (1,0,0)^T \tag{7} $$

$$ {}^0\boldsymbol{x}_{1,i} = \boldsymbol{R}_{z,\alpha} (0,1,0)^T = \left({}^0x_{1,i,x}, {}^0x_{1,i,y}, {}^0x_{1,i,z} \right)^T \tag{8} $$

$$ {}^0\boldsymbol{x}_{2,i} = \boldsymbol{R}_{z,\alpha} (1,0,0)^T = \left({}^0x_{2,i,x}, {}^0x_{2,i,y}, {}^0x_{2,i,z} \right)^T . \tag{9} $$

The rotation matrix $\boldsymbol{R}_{z,\alpha}$ is given by

$$ \boldsymbol{R}_{z,\alpha} = \begin{pmatrix} \cos(\alpha_i) & -\sin(\alpha_i) & 0 \\ \sin(\alpha_i) & \cos(\alpha_i) & 0 \\ 0 & 0 & 1 \end{pmatrix} . \tag{10} $$

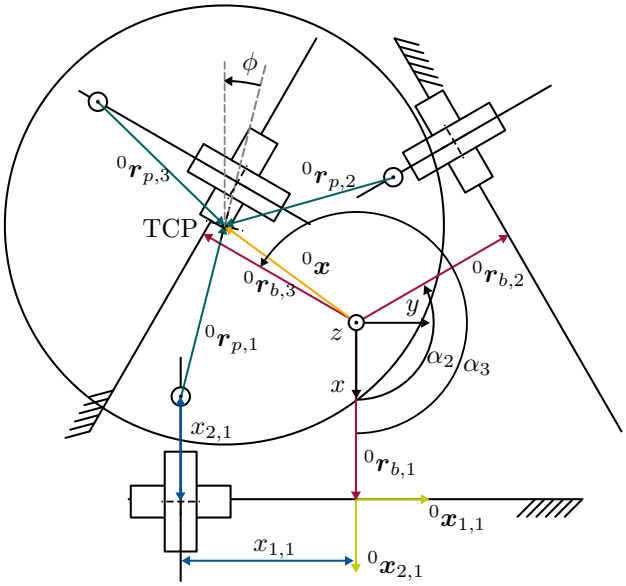


Figure 6. Variables as used for the derivation of the inverse kinematics of the balancing mechanism. All vectors are given in the global COS.

Rearranging to move all constant terms to the left side leads to

$$ {}^0\boldsymbol{x} - {}^0\boldsymbol{r}_{b,i} + {}^0\boldsymbol{r}_{p,i} = x_{1,i} \, {}^0\boldsymbol{x}_{1,i} + x_{2,i} \, {}^0\boldsymbol{x}_{2,i} . \tag{11} $$

The balancing mechanism performs solely planar motions. Thus, the z-components of all vectors in (11) are zero at all times and can be omitted. Conversion to matrix notation leads to the 2×2 constant transformation matrix ${}^0\boldsymbol{A}_i$ of the i^{th} kinematic chain $i = \{1,2,3\}$.

$$ {}^0\boldsymbol{x} - {}^0\boldsymbol{r}_{b,i} + {}^0\boldsymbol{r}_{p,i} = \underbrace{\begin{pmatrix} {}^0x_{1,i,x} & {}^0x_{2,i,x} \\ {}^0x_{1,i,y} & {}^0x_{2,i,x} \end{pmatrix}}_{{}^0\boldsymbol{A}_i} \begin{pmatrix} x_{1,i} \\ x_{2,i} \end{pmatrix} \tag{12} $$

Finally, solving ${}^0x_{1,i,y}$ and ${}^0x_{2,i,x}$ leads to the linear equation system

$$ (x_{1,i}, x_{2,i})^T = {}^0\boldsymbol{A}_i^{-1} \left({}^0\boldsymbol{x} - {}^0\boldsymbol{r}_{b,i} + {}^0\boldsymbol{r}_{p,i} \right) \tag{13} $$

and the desired carriage positions $x_{1,i}$.

4.2. Velocity and Acceleration Analysis

This section is dedicated to the velocity and acceleration analysis of the balancing mechanism. Firstly, the driven carriage's velocities are derived for given TCP translational and rotational velocities. Subsequently, this is repeated for the accelerations.

4.2.1. Velocity Analysis

Differentiation of the loop closure, Equation (5), with respect to time leads to

$$ {}^0\dot{\boldsymbol{x}} = \dot{x}_{1,i}\,{}^0\boldsymbol{x}_{1,i} + \dot{x}_{2,i}\,{}^0\boldsymbol{x}_{2,i} - {}^0\boldsymbol{\omega} \times {}^0\boldsymbol{r}_{p,i}\,, \tag{14} $$

where the vector ${}^0\boldsymbol{\omega} = (0,0,\omega)^T$ describes the rotational velocity of the TCP, i.e., the counterweight. The right-sided scalar product with ${}^0\boldsymbol{x}_{1,i}$ eliminates ${}^0\boldsymbol{x}_{2,i}$ as these two vectors are by definition always being perpendicular to each other, leading to

$$ {}^0\dot{\boldsymbol{x}} \cdot {}^0\boldsymbol{x}_{1,i} = \dot{x}_{1,i} - \left({}^0\boldsymbol{\omega} \times {}^0\boldsymbol{r}_{p,i}\right) \cdot {}^0\boldsymbol{x}_{1,i}\,. \tag{15} $$

Thus, the carriage velocities are given by

$$ \dot{x}_{1,i} = {}^0\dot{\boldsymbol{x}} \cdot {}^0\boldsymbol{x}_{1,i} + \left({}^0\boldsymbol{r}_{p,i} \times {}^0\boldsymbol{x}_{1,i}\right) \cdot {}^0\boldsymbol{\omega}\,. \tag{16} $$

Here, the cross product ${}^0\boldsymbol{r}_{p,i} \times {}^0\boldsymbol{x}_{1,i}$ is given by

$$ {}^0\boldsymbol{r}_{p,i} \times {}^0\boldsymbol{x}_{1,i} = r_p \begin{pmatrix} cos(\alpha+\phi) \\ sin(\alpha+\phi) \\ 0 \end{pmatrix} \times \begin{pmatrix} -sin(\alpha) \\ cos(\alpha) \\ 0 \end{pmatrix} = r_p \begin{pmatrix} 0 \\ 0 \\ cos(\phi) \end{pmatrix} \tag{17} $$

thus

$$ \dot{x}_{1,i} = {}^0\dot{\boldsymbol{x}} \cdot {}^0\boldsymbol{x}_{1,i} + r_p \cdot cos(\phi)\omega\,. \tag{18} $$

4.2.2. Acceleration Analysis

By further differentiation of the loop closure, Equation (5), it follows that

$$ {}^0\ddot{\boldsymbol{x}} = \ddot{x}_{1,i}\,{}^0\boldsymbol{x}_{x,1i} + \ddot{x}_{2,i}\,{}^0\boldsymbol{x}_{2,i} - {}^0\dot{\boldsymbol{\omega}} \times {}^0\boldsymbol{r}_{p,i} - {}^0\boldsymbol{\omega} \times \left({}^0\boldsymbol{\omega} \times {}^0\boldsymbol{r}_{p,i}\right). \tag{19} $$

Due to the design of the balancing mechanism with a large moment of inertia, only small angular velocities, ω, are to be expected; thus, ${}^0\boldsymbol{\omega} \times \left({}^0\boldsymbol{\omega} \times {}^0\boldsymbol{r}_{p,i}\right) = \omega^2\,{}^0\boldsymbol{r}_{p,i}$ is small and can be neglected. Here again, a right-sided scalar product of (19) with ${}^0\boldsymbol{x}_{x,1i}$ is used to eliminate ${}^0\boldsymbol{x}_{2,i}$.

$$ {}^0\ddot{\boldsymbol{x}} \cdot {}^0\boldsymbol{x}_{1,i} = \ddot{x}_{1,i} - \left({}^0\dot{\boldsymbol{\omega}} \times {}^0\boldsymbol{r}_{p,i}\right) \cdot {}^0\boldsymbol{x}_{1,i} \tag{20} $$

Finally, solving for the carriage acceleration leads to

$$ \ddot{x}_{1,i} = {}^0\ddot{\boldsymbol{x}} \cdot {}^0\boldsymbol{x}_{1,i} + \left({}^0\boldsymbol{r}_{p,i} \times {}^0\boldsymbol{x}_{1,i}\right) \cdot {}^0\dot{\boldsymbol{\omega}} \tag{21} $$

$$ = {}^0\ddot{\boldsymbol{x}} \cdot {}^0\boldsymbol{x}_{1,i} + r_p \cdot cos(\phi)\dot{\omega}\,. \tag{22} $$

4.3. Dynamics

The dynamics of the balancing mechanism are needed to calculate the counterweight acceleration required to achieve a desired balancing action, in terms of balancing forces in the x- and y-directions and a balancing moment about the z-axis. Due to the relatively small mass of the linear guide rails (see Table 1), their inertia forces are neglected in the following

calculations. Since all the movements of the balancing mechanism are in the horizontal plane, which is perpendicular to the gravity vector, all the gravitational forces are constant and do not affect the balancing. Therefore, gravitational forces are also neglected in the derivations. The inverse dynamics are calculated using the Newton–Euler equations.

Table 1. Mass properties of the balancing mechanism.

Part	Mass [kg]	Moment of Inertia [kg m^2]
Base including drives	3.445	-
Linear guide rails	0.060	-
Driven carriage	0.249	-
Balancing mass	5.900	0.112

4.3.1. Translational Dynamics

Formulating the equilibrium of forces for the overall system with respect to the attachment point at the center of the base leads to

$$ {}^0\boldsymbol{f} = m_b\, {}^0\ddot{\boldsymbol{x}} + m_c \sum_{i=1}^{3} \ddot{x}_{1,i}\, {}^0\boldsymbol{x}_{1,i}\,. \tag{23} $$

Here, the scalars m_b and m_c stand for the mass of the counterweight and the driven carriages, respectively. The vector ${}^0\boldsymbol{f}$ denotes the reaction forces acting between the balancing mechanism and the robot frame. Substitution of $\ddot{x}_{1,i}$ by (22) leads to

$$ {}^0\boldsymbol{f} = m_b\, {}^0\ddot{\boldsymbol{x}} + m_c \sum_{i=1}^{3} \left({}^0\ddot{\boldsymbol{x}} \cdot {}^0\boldsymbol{x}_{1,i} \right) {}^0\boldsymbol{x}_{1,i} + m_c \cdot r_p \cdot cos(\phi)\dot{\omega} \sum_{i=1}^{3} {}^0\boldsymbol{x}_{1,i}\,. \tag{24} $$

From the symmetry of the balancing mechanism, it follows that $\sum_{i=1}^{3} {}^0\boldsymbol{x}_{1,i} = 0$. Thus, a rotation of the counterweight does not change the total CoM of the balancing mechanism. Therefore,

$$ {}^0\boldsymbol{f} = m_b\, {}^0\ddot{\boldsymbol{x}} + m_c \sum_{i=1}^{3} \left({}^0\ddot{\boldsymbol{x}} \cdot {}^0\boldsymbol{x}_{1,i} \right) {}^0\boldsymbol{x}_{1,i}\,. \tag{25} $$

Rearranging gives

$$ {}^0\boldsymbol{f} = m_b\, {}^0\ddot{\boldsymbol{x}} + m_c \sum_{i=1}^{3} {}^0\boldsymbol{x}_{1,i} \left({}^0\boldsymbol{x}_{1,i}^T\, {}^0\ddot{\boldsymbol{x}} \right) \tag{26} $$

$$ = m_b\, {}^0\ddot{\boldsymbol{x}} + m_c \sum_{i=1}^{3} \left({}^0\boldsymbol{x}_{1,i}\, {}^0\boldsymbol{x}_{1,i}^T \right) {}^0\ddot{\boldsymbol{x}} \tag{27} $$

$$ = \boldsymbol{M}\, {}^0\ddot{\boldsymbol{x}} \tag{28} $$

with

$$ \boldsymbol{M} = \begin{pmatrix} m_b + 1{,}5m_c & 0 & 0 \\ 0 & m_b + 1{,}5m_c & 0 \\ 0 & 0 & m_{b,z} \end{pmatrix}. \tag{29} $$

All components of the balancing mechanism perform purely planar motions, all (dynamic) reaction forces, ${}^0\boldsymbol{f}$, and accelerations, ${}^0\ddot{\boldsymbol{x}}$, lie in the xy-plane. Thus, in the following, the z-components of all vectors and the mass matrix component $m_{b,z}$ can be omitted. Finally, solving for ${}^0\ddot{\boldsymbol{x}}$ leads to the desired transformation from the desired reaction forces to the required counterweight acceleration:

$$ {}^0\ddot{\boldsymbol{x}} = \boldsymbol{M}^{-1}\, {}^0\boldsymbol{f}\,. \tag{30} $$

4.3.2. Rotational Dynamics

The equilibrium of moments about the base center point gives:

$$ {}^0\boldsymbol{t} = {}^{CoM}\boldsymbol{I}_b \, {}^0\dot{\boldsymbol{\omega}} + m_c \sum_{i=1}^{3} \ddot{x}_{1,i} \left({}^0\boldsymbol{r}_{b,i} \times {}^0\boldsymbol{x}_{1,i} \right) + m_b \left({}^0\boldsymbol{x} \times {}^0\ddot{\boldsymbol{x}} \right) \tag{31} $$

with ${}^{CoM}\boldsymbol{I}_b$ being the moment of inertia of the counterweight, measured in a COS fixed at its CoM. The variable ${}^0\boldsymbol{t}$ is defined as the moment acting between the balancing mechanism and the robot frame. Hence, the z-component of ${}^0\boldsymbol{t}$, which is used to balance moments about the z-axis, is given by

$$ {}^0t_z = I_{b,zz}\dot{\omega} + r_b \cdot m_c \sum_{i=1}^{3} \ddot{x}_{1,i} + m_b \left({}^0\boldsymbol{x} \times {}^0\ddot{\boldsymbol{x}} \right). \tag{32} $$

Again, substitution of $\ddot{x}_{1,i}$ by (22) leads to

$$ {}^0t_z = I_{b,zz}\dot{\omega} + 3m_c \cdot r_b \cdot r_p \cdot cos(\phi)\dot{\omega} + r_b \cdot m_c \sum_{i=1}^{3} \left({}^0\ddot{\boldsymbol{x}} \cdot {}^0\boldsymbol{x}_{1,i} \right) + m_b \left({}^0\boldsymbol{x} \times {}^0\ddot{\boldsymbol{x}} \right). \tag{33} $$

Since the scalar product is distributive over vector addition, the latter can be written as

$$ {}^0t_z = I_{b,zz}\dot{\omega} + 3m_c \cdot r_b \cdot r_p \cdot cos(\phi)\dot{\omega} + r_b \, {}^0\ddot{\boldsymbol{x}} \cdot \sum_{i=1}^{3} {}^0\boldsymbol{x}_{1,i} + m_b \left({}^0\boldsymbol{x} \times {}^0\ddot{\boldsymbol{x}} \right). \tag{34} $$

From the symmetry of the balancing mechanism, it follows that $\sum_{i=1}^{3} {}^0\boldsymbol{x}_{1,i} = 0$.

$$ \left(I_{b,zz} + 3m_c r_b r_p cos(\phi) \right)\dot{\omega} = {}^0t_z - m_b \left({}^0\boldsymbol{x} \times {}^0\ddot{\boldsymbol{x}} \right) \tag{35} $$

In the case of the balancing mechanism under consideration, one finds that (c.f. Section 5)

$$ 3m_c r_b r_p = 0.005 \, \mathrm{kg\,m^2} << I_{b,zz} = 0.112 \, \mathrm{kg\,m^2}. \tag{36} $$

Therefore, the term $3m_c r_b r_p cos(\phi)$ can be neglected, leading directly to the desired transformation from the reaction moment to the required counterweight rotational acceleration:

$$ \dot{\omega} = \frac{ {}^0t_z - m_b \left({}^0\boldsymbol{x} \times {}^0\ddot{\boldsymbol{x}} \right)}{I_{b,zz}}. \tag{37} $$

5. Balancing Mechanism Dimensioning

As described in Section 3, the performance of the balancing mechanism presented in this publication is intended to be evaluated on the Suisui Bot, a low-cost Delta robot with a workspace of 0.3 m in diameter and 0.1 m in height. In order to dimension the balancing mechanism used for the evaluation, this section first introduces the evaluation scenario and then presents an analysis of the expected shaking forces and moments. Based on this analysis, the dimensions of the balancing mechanism are determined.

5.1. Evaluation Scenario

The Suisui Bot consist of three identical $\underline{R}(SS)_2$ kinematic chains, connecting the moving platform with the base (see Figure 7). Here, S denotes a spherical joint. These kinematic chains comprise a link connected to the robot's base by an actuated revolute joint, hereinafter referred to as the proximal link and a spatial parallelogram $(SS)_2$. This spatial parallelogram is composed of two parallel connecting rods (denoted as distal links), attached by spherical joints to both the moving platform and the proximal link.

All proximal links are arranged uniformly distributed by an angle of 120° on the base radius r_b, as are the parallelograms connected to the platform with the radius r_p. The lengths of the proximal and distal links are given by the scalars l_p and l_d, respectively. The factors c_p and c_d represent the CoM position along the links in proportion to their length. The Suisui Bot's kinematic parameters, as defined in the production drawings, are summarized in Table 2.

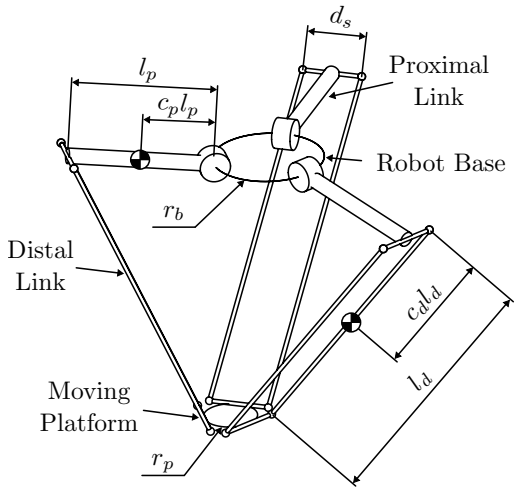


Figure 7. Kinematic parameters of the Suisui Bot.

Table 2. Kinematic parameters of the Suisui Bot. Please refer to Figure 7 for their definition.

Parameter:	l_p **[mm]**	l_d **[mm]**	r_b **[mm]**	r_p **[mm]**	d_s **[mm]**
Value:	178	324	42	36	74

The mass parameters of the Suisui Bot have been determined using a precision scale and compared with the CAD data. These measurements show that the CAD data provide a satisfactory estimate of the masses, e.g., the measured masses of the three proximal link main bodies are 203.5 g, 203.9 g, and 203.4 g, and the weight predicted by the CAD software is 203.4 g. Given these results, the position of the CoM and the moments of inertia of the proximal and distal links are derived directly from a detailed CAD model. The moments of inertia of the actuators, J_a, are taken from the manufacturer's data sheet. All mass parameters are summarized in Table 3.

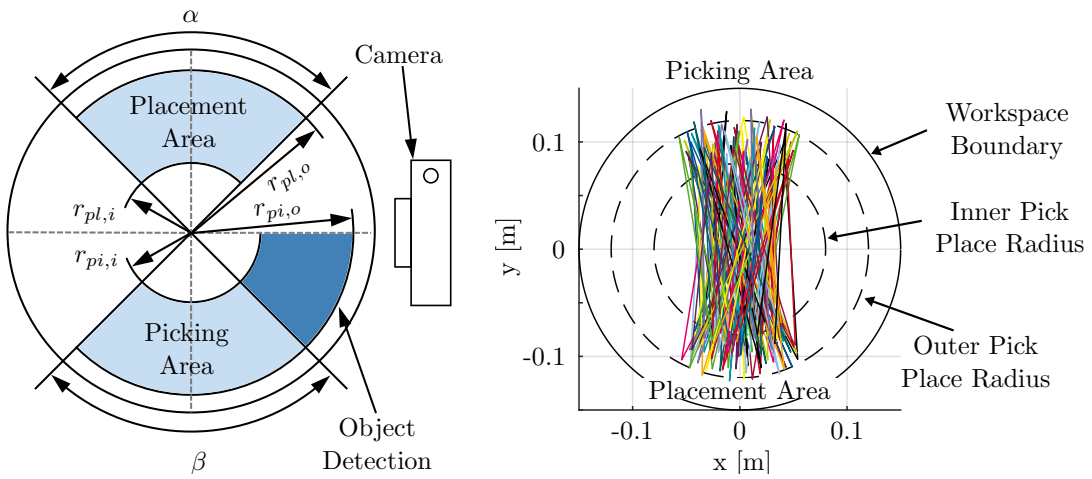
Table 3. Mass and inertia parameters of the Suisui Bot. The moment of inertia of the actuators is specified for the output shaft of the associated gearboxes. The proximal link mass listed here represents the mass of the entire proximal link assembly, including the motor flange.

Parameter:	m_{pl} **[g]**	m_{dl} **[g]**	m_p **[g]**	c_p **[-]**	c_d **[-]**	$J_{pl,yy}$ **[kg m^2]**	$J_{dl,yz}$ **[kg m^2]**	J_a **[kg m^2]**
Value:	331	32	278	0.43	0.5	0.00165	0.00030	0.00662

In order to evaluate the functionality of the balancing mechanism in a realistic setting, a conveyor belt unloading scenario is emulated. This is achieved by placing a turntable beneath the robot and utilizing steel disks as the handling objects (see Figure 5). A vacuum gripper is used for picking. A camera is installed next to the robot to detect the handling objects on the turntable. The turntable has three areas: picking, placement, and object detection (see Figure 8a). These areas are characterized by polar coordinates, represented by their inner ($r_{pl,i}$, $r_{pi,i}$) and outer ($r_{pl,o}$, $r_{pi,o}$) radii and angles (α, β). Within these areas, the pick-and-place positions and the motion times are varied using the quasi-randomized Halton sequence (cf. [28,29]). The trajectories are based on an Adept cycle with 25 mm up and down stroke. The horizontal translation is defined by the pick-and-place positions. Following [6], the geometric path is smoothed at the transitions with Lamé curves and combined with a 4-5-6-7 polynomial motion profile.

For all experiments, the inner radii $r_{pl,i}$ and $r_{pi,i}$ are set to 0.08 m and the outer radii $r_{pl,o}$ and $r_{pi,o}$ are set to 0.125 m in order to obtain adequate horizontal motion and to prevent handling objects from falling off the turntable. The minimum motion time from the pick to the

place position is 0.2 s, but due to the latency of the vacuum gripper no objects can be handled at this speed. Therefore, for experimental validation, the motion time from the pick to the place position is defined to be between 0.25 s and 0.3 s. Exemplary trajectories recorded in pick-and-place experiments with angles α and β both set to 60° can be seen in Figure 8b.



(**a**) Layout of the turntable

(**b**) Trajectories generated using a Halton sequence for process variation

Figure 8. (**a**) shows the sectioning of the turntable as used for the trajectory planning. (**b**) shows a set of 75 trajectories defined by a Halton sequence and recorded in experiments.

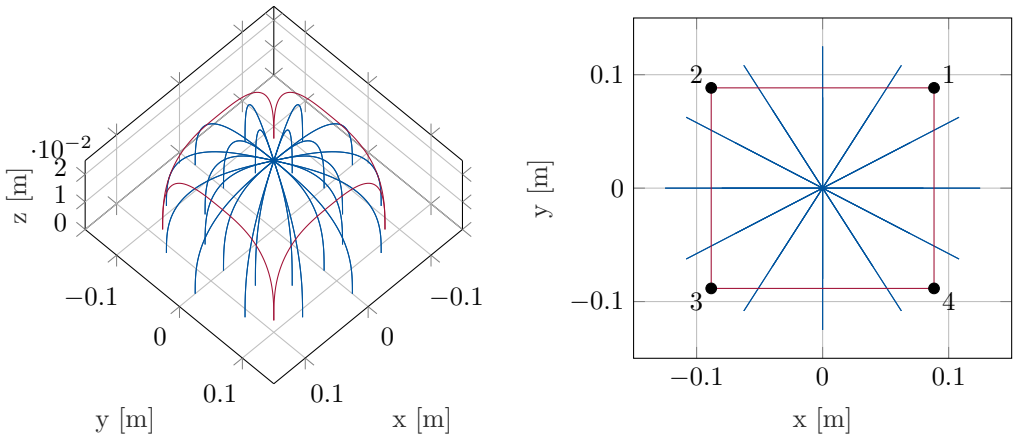
5.2. Shaking Force and Shaking Moment Analysis

In order to define the dimensional parameters of the balancing mechanism, the highest shaking forces and moments that could occur in this scenario were analyzed. For this purpose, 16 trajectories were defined, covering the entire turntable area. Twelve of them are arranged in an asterisk pattern. Six of them have a horizontal translation of 0.25 m and the motion time from the pick to the place position is set to its minimum value of 0.2 s, resulting in a maximum acceleration of approximately 76 m s^{-2}. The remaining six trajectories have a horizontal translation of 0.16 m, and a motion time of 0.18 s in order to obtain the same peak TCP acceleration. Finally, four trajectories are in the shape of the largest square that fits into a circle with a radius of 0.125 m as $r_{pl,o}$ and $r_{pi,o}$. This square is parallel to the x-axis and y-axis. The motion time for these trajectories is set to 0.184 s to obtain the same peak acceleration as for the other trajectories. As for the practical experiments, these trajectories are based on an Adept cycle with 25 mm up and down stroke, and the geometric path is smoothed with Lamé curves and combined with a 4-5-6-7 polynomial motion profile.

The resulting trajectories are shown in Figure 9. In the case of the trajectories arranged in an asterisk pattern, the most critical ones are those where the robot moves along one of its kinematic chains (e.g., along the x-axis). In the case of the trajectories arranged in a square, the most critical ones are those where the robot moves from point 1 to point 2 or from point 3 to point 4 (see Figure 9a). Due to the symmetry of the robot, the shaking forces on these trajectories are equal. The maximum shaking forces and moments calculated on the basis of these critical cases for the asterisk and square trajectories are summarized in Table 4. The calculation was performed according to the mass parameters of the Suisui Bot.

Table 4. Maximum shaking forces and moments calculated for the critical cases for the trajectories in an asterisk and in a square pattern.

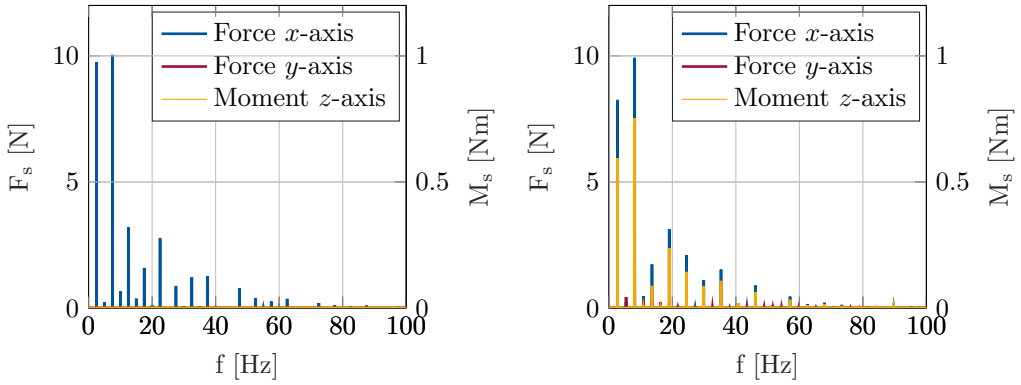
Trajectory	Maximal Shaking Force	Maximal Shaking Moment
Asterisk	42.3 N	0 Nm
Square	41.1 N	2.99 Nm



(**a**) Side view (**b**) Top view

Figure 9. Trajectories used to access the maximum shaking forces and moments.

Figure 10 shows a Fourier transform of the relevant shaking forces and moments caused by the most critical trajectories in both an asterisk and a square arrangement. The dominant frequencies are below 10 Hz, with a significant share of the relevant frequency components extending to approximately 50 Hz.



(**a**) Asterisk (**b**) Square

Figure 10. Fourier transform of the shaking forces and moments calculated for the critical cases for the trajectories in an asterisk and a square pattern.

5.3. Dimensioning

In typical pick-and-place scenarios, the robot picks up a payload on one side of the workspace, transports it to the opposite side, places it, and returns unloaded. This unidirectional mass transport results in a one-sided movement of the counterweight when both the shaking forces caused by the robot and the payload are compensated by active balancing [11,22]. As a result, the counterweight can reach its motion limits. To counteract this effect, a centering algorithm has been defined and presented in [30]. However, since any acceleration required to bring the counterweight back to center causes a shaking force on the frame, it is desirable to have sufficient permissible counterweight travel to allow for smooth and slow centering actions.

With this in mind, the dimensions of the counterweight were chosen so that the Suisui Bot could be dynamically balanced at least twice in the same direction on the paths with the highest shaking forces and moments without returning to the center of the balancing mechanism's workspace. To calculate the required counterweight mass and inertia, the kinematic parameters r_b and r_p had to be defined first. Their choice is based solely on geometric constraints and was chosen to achieve the maximum counterweight travel and mechanism size that would fit on the Suisui Bot. This resulted in $r_b = 0.081$ m and $r_p = 0.087$ m. The control hardware for the robot and balancing unit is mounted on the top of the frame. This limits

the radius of the counterweight. The mass characteristics of the mechanism are summarized in Table 1. The mechanism is driven by Nanotec Electronic GmbH & Co. KG (Feldkirchen, Germany) *ST4118D3004* stepper motors (0.80 Nm holding torque, 92 W output power).

Given these dimensions, the maximum power consumption, counterweight speed, and motion (calculated according to Section 4.3) for the two most critical trajectories are summarized in Table 5, along with the maximum required travel, $x_{1,i}$, of the balancing mechanism actuators. For comparison, the permissible travel is ± 50 mm. It should be noted that the calculated power consumption does not include any mechanical or electrical losses, such as the friction caused by the plain bearings in the linear guides and the lead screw.

Table 5. Power requirements and CoM motion of the balancing mechanism.

Trajectory	Maximal Power	Maximal Velocity		Maximal Position		Maximal $x_{1,i}$
		xy-Plane	ϕ	(xy)-Plane	ϕ	
Asterisk	4.4 W	0.241 m s^{-1}	0 rad s^{-1}	0.021 m	0 rad	0.0185 m
Square	4.4 W	0.197 m s^{-1}	0.84 rad s^{-1}	0.015 m	0.062 rad	0.0186 m

6. Summary and Discussion

This publication presented the design of a novel three-DoF planar parallel mechanism for the dynamic balancing of Delta robots. First, the main design requirements for a balancing mechanism were defined, and possible mechanisms were presented based on these requirements. Finally, a 3-$\underline{P}PR$ mechanism was identified as one of the most promising solutions given the following:

- its small footprint, which allows it to be mounted directly on the robot, resulting in direct force/moment transmission;
- its low weight, due to the use of a counterrotating counterweight;
- its low height, which makes it possible to minimize parasitic shaking moments;
- its, to a good approximation, linear kinematics and dynamics.

To evaluate the performance of the mechanism, a small, low-cost prototype was built and tested on the low-cost Delta robot Suisui Bot. A description of the control system and an experimental validation of the overall system is beyond the scope of this publication, but can be found in [19,30]. In these publications, it has been shown that, in a scenario with 75 quasi-randomized pick-and-place positions and cycle times as described in Section 5, the mechanism provides a significant vibration reduction of up to 86% [19]. In future work, concepts for combining this mechanism with solutions for balancing the shaking moments about the x- and y-axes will be investigated, as these represent the highest shaking moments. A combination with gyroscopes seems promising to achieve high moments with minimal additional mass and inertia.

Author Contributions: Investigation and writing, C.M.; review and supervision, M.H., Y.T. and B.C. All authors have read and agreed to the published version of the manuscript.

Funding: This work was supported by the DAAD with funds from the German Foreign Office.

Data Availability Statement: The original contributions presented in the study are included in the article; further inquiries can be directed to the corresponding author.

Conflicts of Interest: The authors declare no conflicts of interest.

Abbreviations

The following abbreviations are used in this manuscript:

CoM	Center of Mass
COS	Coordinate System
TCP	Tool Center Point

Appendix A

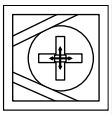
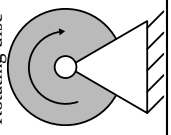
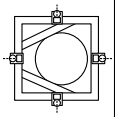
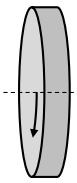
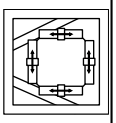
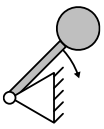
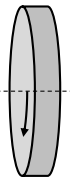
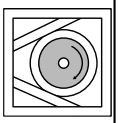
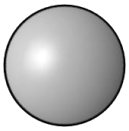
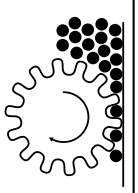
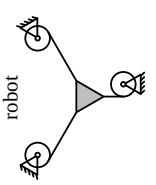
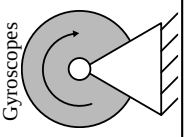
Solution Concepts	Subfunctions: Force Balancing (FB)			Subfunctions: Moment Balancing (MB)			Subfunctions: Combination of FB and MB
	Principle mechanism	Combination	Attachment to the robot	Principle mechanism	Combination	Attachment to the robot	
1	Linear slider 	Separate balancing mechanisms	One mechanism at the center of the robot 	Rotating disc 	Separate balancing mechanisms	Off-centered duplicate mechanisms 	Separate counter weight and counter rotating inertia
2	Counter rotating eccentric masses 	Attach the mechanism to a rotary table 	Off-centered duplicate mechanisms 	Pendulum 	Attach the mechanism to a rotary table 	One mechanism at the center of the robot 	Counter rotating counter weight
3	Slider-crank linkage 	Serial combination of balancing mechanisms		Rotating sphere 	Serial combination of balancing mechanisms	Intersection between the counter rotating inertias	
4	Moving steel balls or fluids 			Agile Eye 3-RRR spherical parallel manipulator [GH94]			
5	Cable- driven parallel robot 			Gyroscopes 			

Figure A1. Page one of the morphological matrix containing solution candidates for the functions of the dynamic balancing task. For simplicity, solutions that can be used for both force and moment balancing are only listed under subfunction force balancing [31].

Solution Concepts	Subfunctions							
	Force Balancing (FB)			Moment Balancing (MB)			Combination of FB and MB
	Principle mechanism	Combination	Attachment to the robot	Principle mechanism	Combination	Attachment to the robot	
5	Planar parallel 3-RRR mechanism						
7	Planar parallel 3-RPR mechanism						
8	Planar parallel 3-PPR mechanism						
9	Planar parallel 3-PRP mechanism						
10	Planar parallel 2-RRP mechanism						

Figure A2. Page two of the morphological matrix containing solution candidates for the functions of the dynamic balancing task. For simplicity, solutions that can be used for both force and moment balancing are only listed under subfunction force balancing.

Solution Concepts	Subfunctions								
	Force Balancing (FB)			Moment Balancing (MB)			Combination of FB and MB		
	Principle mechanism	Combination	Attachment to the robot	Principle mechanism	Combination	Attachment to the robot			
11	Five-bar linkage								
12	Delta robot								
13	Stewart platform								
14									
15									

Figure A3. Page three of the morphological matrix containing solution candidates for the functions of the dynamic balancing task. For simplicity, solutions that can be used for both force and moment balancing are only listed under subfunction force balancing.

References

1. Siciliano, B.; Khatib, O. *Springer Handbook of Robotics*, 2nd ed.; Springer: Berlin/Heidelberg, Germany, 2016.
2. van der Wijk, V.; Herder, J.L. Dynamic Balancing of Clavel's Delta Robot. In *Computational Kinematics*; Kecskeméthy, A., Müller, A., Eds.; Springer: Berlin/Heidelberg, Germany, 2009; Volume 3, pp. 315–322.
3. Lowen, G.G.; Berkof, R.S. Survey of Investigations into the Balancing of Linkages. *J. Mech.* **1968**, *3*, 221–231. [CrossRef]
4. Cheng, H.; Liu, F.; Li, W.; Hao, L. Vibration Measurement, Analysis and Dynamic Parameter Optimization for Delta Robot. In Proceedings of the 2017 IEEE 7th Annual International Conference on CYBER Technology in Automation, Control, and Intelligent Systems (CYBER), Piscataway, NJ, USA, 31 July–4 August 2017; pp. 809–814. [CrossRef]
5. Barnard, C.J.; Briot, S.; Caro, S. Trajectory Generation for High Speed Pick and Place Robots. In *Proceedings of the ASME 11th Biennial Conference on Engineering Systems Design and Analysis. Volume 3: Advanced Composite Materials and Processing; Robotics; Information Management and PLM; Design Engineering. Nantes, France*; American Society of Mechanical Engineers: New York, NY, USA, 2012; pp. 165–174. [CrossRef]
6. Gauthier, J.F.; Angeles, J.; Nokleby, S. Optimization of a Test Trajectory for SCARA Systems. In *Advances in Robot Kinematics*; Lenarcic, J., Philippe, W., Eds.; Springer: Berlin/Heidelberg, Germany, 2008; Volume 18, pp. 225–234.
7. Nenchev, D.N.; Yoshida, K.; Vichitkulsawat, P.; Uchiyama, M. Reaction Null-Space Control of Flexible Structure Mounted Manipulator Systems. *IEEE Trans. Robot. Autom.* **1999**, *15*, 1011–1023. [CrossRef]
8. Singer, N.C.; Seering, W.P. Preshaping Command Inputs to Reduce System Vibration. *J. Dyn. Syst. Meas. Control* **1990**, *112*, 76–82. [CrossRef]
9. Singhose, W.; Singer, N.; Seering, W. Comparison of Command Shaping Methods for Reducing Residual Vibration. In Proceedings of the European Control Conference, Roma, Italy, 5–8 September 1995; pp. 1126–1131.
10. Auer, T.; Kronthaler, P.; Woittennek, F. Optimalsteuerungsentwurf für ein elastisch gekoppeltes Flächenportal mit Vergleich zu Standardverfahren. In *Siebte IFToMM D-A-CH Konferenz 2021*; Online-Konferenz; IFToMM D-A-CH, Universität Duisburg-Essen: Duisburg, Germany, 2021. [CrossRef]
11. van der Wijk, V.; Herder, J.L. Active Dynamic Balancing Unit for Controlled Shaking Force and Shaking Moment Balancing. In Proceedings of the Volume 2: 34th Annual Mechanisms and Robotics Conference, Montreal, QC, Canada, 15–18 August 2010; pp. 1515–1522.
12. Wang, K.; Li, K.; Zhang, Q.; Luo, M.; Chen, P. Enhanced Active Dynamic Balancing of the Planar Robots Using a Three-Rotating-Bar Balancer. *Adv. Mech. Eng.* **2016**, *8*, 1687814016643885. [CrossRef]
13. Wei, B.; Zhang, D. A Review of Dynamic Balancing for Robotic Mechanisms. *Robotica* **2021**, *39*, 55–71. [CrossRef]
14. van der Wijk, V. Actively Dynamically Balanced Robot Manipulator. Available online: https://kineticart.nl/en/collection_of_works/scientific_work_on_mechanisms_and_robotics/actively_dynamically_balanced_robot_manipulator_2010 (accessed on 22 August 2022).
15. Raaijmakers, R. Besi zoekt snelheidslimiet pakken en plaatsen op. *Mechatronica Machinebouw*, 11 September 2007, 26–31.
16. Wang, K.; Luo, M.; Mei, T.; Zhao, J.; Cao, Y. Dynamics Analysis of a Three-DOF Planar Serial-Parallel Mechanism for Active Dynamic Balancing with Respect to a Given Trajectory. *Int. J. Adv. Robot. Syst.* **2013**, *10*, 23. [CrossRef]
17. Verein deutscher Ingenieure. *VDI 2221: 2019-11—Design of Technical Products and Systems: Model of Product Design Part 1*; Technical Report; Beuth Verlag GmbH: Berlin, Germany, 2019.
18. Pahl, G.; Beitz, W.; Feldhusen, J.; Grote, K.H. *Engineering Design, a Systematic Approach*, 3rd ed.; Springer: London, UK, 2007.
19. Mirz, C.J. Development of an Active Dynamic Balancing Unit for Pick and Place Applications. Ph.D. Thesis, Rheinisch-Westfälische Technische Hochschule Aachen, Aachen, Germany, 2023. [CrossRef]
20. van der Wijk, V.; Herder, J.L. Guidelines for Low Mass and Low Inertia Dynamic Balancing of Mechanisms and Robotics. In *Advances in Robotics Research*; Kröger, T., Wahl, F.M., Eds.; Springer: Berlin/Heidelberg, Germany, 2009; pp. 21–30. [CrossRef]
21. Lanchester, F.W. Engine Balancing. In *The Horseless Age*; Ingersoll, E.P., Ed.; Horseless Age Company: New York, NY, USA, 1914; Volume 12, pp. 494–495.
22. van der Wijk, V.; Herder, J.L. Force Balancing of Variable Payload by Active Force-Balanced Reconfiguration of the Mechanism. In Proceedings of the 2009 ASME/IFToMM International Conference on Reconfigurable Mechanisms and Robots, New York, NY, USA, 22–24 June 2009.
23. THK. Optimal THK Unit, CATALOG No.427-2. Available online: https://www.thk.com/jp/ja/products/catalog/ctr/427_unit.pdf (accessed on 28 July 2024).
24. Eidelberg, B. Integrated Large XY Rotary Positioning Table with Virtual Center of Rotation. U.S. Patent, US8104752B2, 31 January 2012
25. Kimura, Y. Tilt Stage (Patent Application). Japan Patent, JP2010234498A, 10 September 2010.
26. Kerle, H.; Corves, B.; Hüsing, M. *Getriebetechnik: Grundlagen, Entwicklung und Anwendung ungleichmäßig übersetzender Getriebe*, 5., überarbeitete und erweiterte auflage ed.; Lehrbuch, Springer Vieweg: Wiesbaden, Germany, 2015.
27. Mirz, C.; Hüsing, M.; Takeda, Y.; Corves, B. Low Cost Delta Robot for the Experimental Validation of Frame Vibration Reduction Methods. In *ROMANSY 24—Robot Design, Dynamics and Control*; CISM International Centre for Mechanical Sciences; Springer International Publishing: Cham, Switzerland, 2022; Volume 606, pp. 332–339. [CrossRef]
28. Halton, J.H. On the Efficiency of Certain Quasi-Random Sequences of Points in Evaluating Multi-Dimensional Integrals. *Numer. Math.* **1960**, *2*, 84–90. [CrossRef]

29. Vandewoestyne, B.; Cools, R. Good Permutations for Deterministic Scrambled Halton Sequences in Terms of L2 -Discrepancy. *J. Comput. Appl. Math.* **2006**, *189*, 341–361. [CrossRef]
30. Mirz, C.; Hüsing, M.; Takeda, Y.; Corves, B. Active Dynamic Balancing of Delta Robots in Pick and Place Tasks. In *Advances in Mechanism and Machine Science*; Okada, M., Ed.; Springer: Cham, Switzerland, 2023; Voluem 148, pp. 255–265. [CrossRef]
31. Gosselin, C.M.; Hamel, J.F. The Agile Eye: A High-Performance Three-Degree-of-Freedom Camera-Orienting Device. In Proceedings of the 1994 IEEE International Conference on Robotics and Automation, San Diego, CA, USA, 8–13 May 1994; pp. 781–786. [CrossRef]

Disclaimer/Publisher's Note: The statements, opinions and data contained in all publications are solely those of the individual author(s) and contributor(s) and not of MDPI and/or the editor(s). MDPI and/or the editor(s) disclaim responsibility for any injury to people or property resulting from any ideas, methods, instructions or products referred to in the content.